Regularization for improving the deconvolution in real-time near-field acoustic holography

Sébastien Paillasseur, Jean-Hugh Thomas,[a] and Jean-Claude Pascal
Laboratoire d'Acoustique de l'Université du Maine (LAUM Unité Mixte de Recherche-CNRS 6613), avenue O. Messiaen, 72085 Le Mans Cedex 09, France

(Received 23 September 2010; revised 12 April 2011; accepted 13 April 2011)

Near-field acoustic holography is a measuring process for locating and characterizing stationary sound sources from measurements made by a microphone array in the near-field of the acoustic source plane. A technique called real-time near-field acoustic holography (RT-NAH) has been introduced to extend this method in the case of nonstationary sources. This technique is based on a formulation which describes the propagation of time-dependent sound pressure signals on a forward plane using a convolution product with an impulse response in the time-wavenumber domain. Thus the backward propagation of the pressure field is obtained by deconvolution. Taking the evanescent waves into account in RT-NAH improves the spatial resolution of the solution but makes the deconvolution problem "ill-posed" and often yields inappropriate solutions. The purpose of this paper is to focus on solving this deconvolution problem. Two deconvolution methods are compared: one uses a singular value decomposition and a standard Tikhonov regularization and the other one is based on optimum Wiener filtering. A simulation involving monopoles driven by nonstationary signals demonstrates, by means of objective indicators, the accuracy of the time-dependent reconstructed sound field. The results highlight the advantage of using regularization and particularly in the presence of measurement noise.
 [DOI: 10.1121/1.3586790]

PACS number(s): 43.60.Sx, 43.60.Pt, 43.60.Gk [EJS] Pages: 3777–3787

I. INTRODUCTION

Many industrial acoustic sources generate nonstationary signals (engine run-ups, wind- screen wiper noise, impact noise, etc.). Sometimes the frequency content of the acoustic signals fluctuates in time. Though the necessity to precisely locate and characterize the sources is often requested even and particularly when the sources cannot be considered as stationary. Nearfield acoustic holography (NAH) is an imaging technique very suitable for recovering the sound field of an acoustic system when the signals emmited by the sources are stationary.[1] When the statistical components of the signals are time-evolving, the standard method is unsuitable. However some adjustments were made on standard NAH to take into account nonstationary acoustic fields. The "time domain holography" method proposed by Hald aims at reconstructing the time pressure signals directly on the source plane on a virtual grid facing the microphone array used for the measurements.[2–4] The method requires several iterations of standard NAH, one for each spectral line and is particularly suitable for studying a short time event. La Rochefoucauld *et al.*[5] implemented this method using discrete Fourier transforms (DFT) and investigated both forward[6] and backward propagation. The regularization parameter used to solve the inverse problem was set by the *L*-curve[7] approach for each spectral line before returning to the time domain.[5] To circumvent the aliasing errors which appear when the sound pressure radiated by an impacted plate is truncated by the use of discrete Fourier transforms, Blais and Ross proposed an implementation based on numerical Laplace transforms (using DFT).[8,9] A similar use of the Laplace transform had been suggested by Wu *et al.* and associated with a propagator described with spherical harmonics.[10] The authors assumed the presence of spherical sources to reconstruct transient acoustic fields by means of Helmholtz equation least squares method. Another method dedicated to fluctuating sources provides a time-dependent map of the spatial pressure field for a chosen frequency.[11] This moving average method can be seen as several iterations of standard NAH, one for each time sample. The method is based on the use of the short time Fourier transform and so, has the advantage to provide a time-continuous field reconstruction.

The disadvantage comes also from this time-processing tool for which the spread of the window is not relevant for each frequency component and has to be set up at the beginning of the analysis. A recent method provides the advantages of both previous methods.[12,13] Real-time nearfield acoustic holography (RT-NAH) indeed allows one to continuously reconstruct the pressure field on the source plane and provides also time-dependent pressure signals on this plane. One specificity of the method is that it does not work in the frequency domain. It is based on inverting, in the time-wavenumber domain, a direct formulation,[14] proposed by Forbes *et al.* and revisited in Ref.15 which gives the time-dependent wavenumber spectrum in a forward plane from the time-dependent wavenumber spectrum acquired in a measurement plane in the near-field of the sources.

[a]Author to whom correspondence should be addressed. Electronic mail: jean-hugh.thomas@univ-lemans.fr

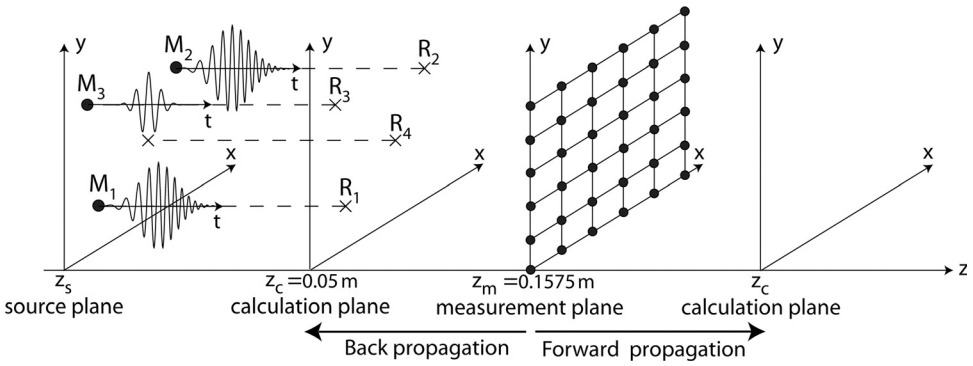

FIG. 1. Geometry of interest. Forward and backward propagation in real-time near-field acoustic holography. The distances between the measurement plane and the calculation plane in both configurations are the same.

The aim of the paper is to show how the inverse process of the real-time nearfield acoustic holography method can be enhanced using a singular value decomposition coupled with regularization techniques which are proved to be effective in standard NAH.[16] Section II summarizes the theoretical background of RT-NAH. Section III describes the problem to solve in NAH in the case of nonstationary sources, which leads to invert an impulse response. Two methods are proposed for this purpose. The first one uses a singular value decomposition and a Tikhonov regularization[16] whose parameter is found by general crossed validation.[7] The second approach for inverting the response is that studied in Ref.12 based on inverse Wiener filtering of an impulse response preprocessed according to Ref. 15. Both methods are applied to a simulation case involving three monopoles driven by nonstationary signals. The presentation of the results obtained is reported in Sec. IV. The two methods are compared using objective indicator values computed from reconstructed time signals. The influence of a measurement noise is also studied. The discussion concludes on the advantage of the use of regularization to enhance the reconstruction sound field in the simulation test presented.

II. REAL-TIME NEARFIELD ACOUSTIC HOLOGRAPHY

A. Forward propagation

The direct problem[15,17] of real-time near-field acoustic holography consists in describing the propagation of the time-dependent sound pressure field measured on a plane $z = z_m$ to a forward calculation plane $z = z_c$ as shown in Fig. 1 ($z_m < z_c$). This can be done by using a convolution product between the measured time-dependent wavenumber spectrum $P(k_x, k_y, z_m, t)$ and an impulse response $h(k_x, k_y, \Delta z, t)$ where $\Delta z = z_c - z_m$ is the propagation distance. Thus the propagated time-dependent wavenumber spectrum $P(k_x, k_y, z_c, t)$ is obtained by

$$P(k_x, k_y, z_c, t) = P(k_x, k_y, z_m, t) * h(k_x, k_y, \Delta z, t), \quad (1)$$

where k_x and k_y are the wavenumbers along x axis and y axis. The time-dependent wavenumber spectrum $P(k_x, k_y, z, t)$ is calculated by applying a two dimensional Fourier transform along x axis and y axis to the sound pressure field $p(x, y, z, t)$,

$$P(k_x, k_y, z, t) = \int_{-\infty}^{+\infty}\int_{-\infty}^{+\infty} p(x, y, z, t) e^{j(k_x x + k_y y)} dx dy. \quad (2)$$

The impulse response $h(k_x, k_y, \Delta z, t)$ introduced in Eq. (1) is obtained by solving the two dimensional Fourier transform of the wave equation

$$\frac{\partial^2 P(k_x, k_y, z, t)}{\partial z^2} - \frac{1}{c^2}\frac{\partial^2 P(k_x, k_y, z, t)}{\partial t^2} - \left(k_x^2 + k_y^2\right) \times P(k_x, k_y, z, t) = 0, \quad (3)$$

where c [ms^{-1}] is the sound speed. With the following substitutions

$\tau = \Delta z/c$ for the propagation delay,

$\Omega_r = ck_r = c\sqrt{k_x^2 + k_y^2}$ for the transition angular frequency, the expression of the impulse response yields

$$h(\Omega_r, \tau, t) = \delta(t - \tau) - \tau\Omega_r \frac{J_1\left(\Omega_r\sqrt{t^2 - \tau^2}\right)}{\sqrt{t^2 - \tau^2}} \Gamma(t - \tau), \quad (4)$$

with J_1 as the Bessel function of the first kind and order 1, $\delta(t)$ as the Dirac delta function and $\Gamma(t)$ as the Heaviside function. An example of this impulse response is presented in Fig. 2. Using the expression of the impulse response in Eq. (1), it is then possible to obtain the time-dependent wavenumber spectrum on the forward calculation plane $P(k_x, k_y, z_c, t)$. The instantaneous spatial pressure in the forward plane $p(x, y, z_c, t)$ is finally determined by applying the

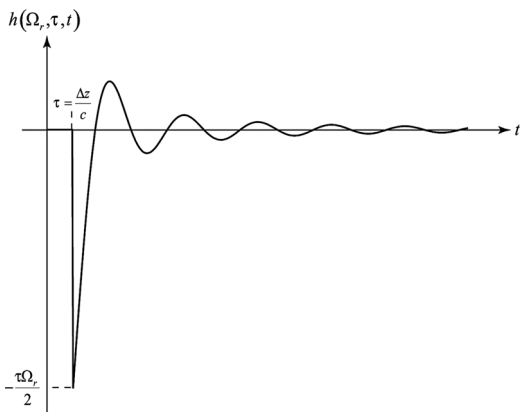

FIG. 2. Impulse response $h(\Omega_r, \tau, t)$.

inverse two dimensional Fourier transform to $P(k_x, k_y, z_c, t)$, which gives a time-evolving description of the sound pressure field on the forward calculation plane.

B. Backward propagation

The goal of real-time near-field acoustic holography is to characterize a source plane composed of nonstationary sound sources. It is thus necessary to obtain the time-dependent pressure field on the source plane from measurements made by a microphone array in the near-field of the source plane. According to Fig. 1, when the calculation plane $z = z_c$ is backward ($z_m > z_c$), the time-dependent wavenumber spectrum $P(k_x, k_y, z_m, t)$ from the measurement plane $z = z_m$ is given by

$$P(k_x, k_y, z_m, t) = P(k_x, k_y, z_c, t) * h(k_x, k_y, z_m - z_c, t). \quad (5)$$

As the propagation distance $z_m - z_c$ in the backward configuration ($z_m > z_c$) is the same as that denoted Δz in the forward configuration ($z_m < z_c$) in Eq. (1), Eq. (5) can be rewritten as

$$P(k_x, k_y, z_m, t) = P(k_x, k_y, z_c, t) * h(k_x, k_y, \Delta z, t). \quad (6)$$

Thus the back-propagated sound pressure field in $z = z_c$ radiated by nonstationary sources is described by the deconvolution problem of Eq. (6), which can be written as

$$P(k_x, k_y, z_c, t) = P(k_x, k_y, z_m, t) * h^{-1}(k_x, k_y, \Delta z, t). \quad (7)$$

In the case of near-field acoustic holography which describes the radiation of stationary sound sources for a particular angular frequency $\omega = 2\pi f$, the formulation of forward propagation ($z_m > z_c$) is given by

$$P(k_x, k_y, z_m, \omega) = P(k_x, k_y, z_c, \omega) H(\Omega_r, \tau, \omega), \quad (8)$$

where the propagator $H(\Omega_r, \tau, \omega)$ is defined as

$$H(\Omega_r, \tau, \omega) = \begin{cases} e^{-j\tau}\sqrt{\omega^2 - \Omega_r^2} & \text{for } \omega \geq \Omega_r \\ e^{-\tau}\sqrt{\Omega_r^2 - \omega^2} & \text{for } \omega < \Omega_r \end{cases}. \quad (9)$$

From Eq. (9), the theoretical frequency response of the inverse impulse response is

$$H^{-1}(\Omega_r, \tau, \omega) = \frac{1}{H(\Omega_r, \tau, \omega)} = \begin{cases} e^{j\tau}\sqrt{\omega^2 - \Omega_r^2} & \text{for } \omega \geq \Omega_r \\ e^{\tau}\sqrt{\Omega_r^2 - \omega^2} & \text{for } \omega < \Omega_r \end{cases}. \quad (10)$$

As shown in Fig. 3, where $\Omega_r/2\pi$ is, for example, set to 0.4 $f_{\max}$ [$f_{\max} = \min(f_s/2, c/2a)$ with f_s as the sampling frequency and a, as the step size between two microphones], the backpropagation acts differently depending on the frequency of the components:

(1) The components with a frequency $f \geq \Omega_r/2\pi$ correspond to the propagating waves. The backpropagation of the propagating waves leads to a change of phase but their amplitudes remain unchanged.

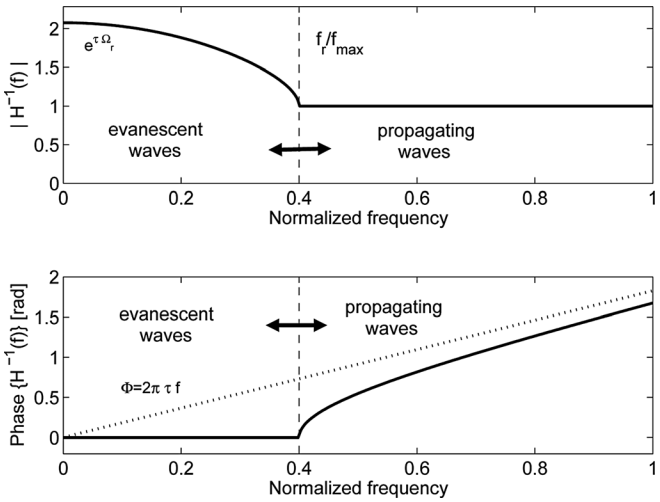

FIG. 3. Modulus and phase of the theoretical Fourier transform of the inverse impulse response $H^{-1}(\Omega_r, \tau, f)$ with $f_{\max} = f_s/2$, where f_s is the sampling frequency.

(2) The components with a frequency $f < \Omega_r/2\pi$ correspond to the evanescent waves. The backpropagation of the evanescent waves leads to an amplification of their amplitudes but their phases remain unchanged. In the presence of measurement noise this amplification may induce erroneous values during backpropagation. The problem is said "ill-posed" and requires specific processing in order to obtain satisfactory solutions. It is important to note that this separation between propagating and evanescent waves is impossible in the case of real-time near-field acoustic holography as the advantage of this method is to remain in the time-wavenumber domain during all the process.

III. SOLVING THE BACKWARD PROPAGATION

Several methods[1,18,19] based on selective filtering in the wavenumber spectrum have been introduced to solve the inverse problem of near-field acoustic holography, however those methods are not suitable in the case of real-time near-field acoustic holography mainly due to the fact that the separation between the propagating and evanescent waves is not possible in the time-wavenumber domain.

A. The impulse response

Sampling the impulse response $h(\Omega_r, \tau, t)$ of Eq. (4) is a delicate point of real-time near-field acoustic holography. Indeed, directly sampling the impulse response, which is designated by direct method, may lead to distortion even if the sampling rate is relatively high. This is due to the fact that the impulse response is defined by an analytical formulation and thus has an infinite frequency band. Oversampling the impulse response may reduce these distortions but the impulse response obtained is not satisfactory. Three processing methods suggested by Grulier *et al.*[15] are applied to the theoretical impulse response in order to improve its frequency response:

Average method. This method consists in average sampling the impulse response instead of directly sampling it. The values of $h(\Omega_r, \tau, t)$ at the time $t = n\Delta t$ are replaced by the mean value $\overline{h}(\Omega_r, \tau, n\Delta t)$ computed on the interval Δt centered at $t = n\Delta t$

$$\overline{h}(\Omega_r,\tau,n\Delta t)=\frac{1}{\Delta t}\int_{n\Delta t-\frac{\Delta t}{2}}^{n\Delta t+\frac{\Delta t}{2}}h(\Omega_r,\tau,t)dt. \tag{11}$$

Chebyshev filtering. A low-pass Chebyshev filter with a cutoff frequency $f_c=6400$ Hz is applied to the impulse response. It is achieved by upsampling the impulse response by a factor $D=8$, using the low-pass filter and then downsampling the resulting response by the factor $1/D$.

Numerical Kaiser filtering. A low-pass Kaiser-Bessel filter with a cutoff frequency $f_c=6640$ Hz is applied to the impulse response. An upsampling factor of $D=2$ is used and the integral for the convolution is numerically computed using the trapezoidal method.

B. Regularization method

The first deconvolution method used is based on the standard Tikhonov regularization[20] which consists in adding a constraint on the solution, in this case the minimization of the solution's energy. The choice of the regularization method is done as it does not require any assumption on the processed signal. The starting point of this deconvolution method is to rewrite, for each point $\left(k_{x_i},k_{y_j}\right)$ of the wavenumber domain, the direct problem

$$P\left(k_{x_i},k_{y_j},z_m,t\right)=P\left(k_{x_i},k_{y_j},z_c,t\right)*h\left(k_{x_i},k_{y_j},\Delta z,t\right), \tag{12}$$

into a matrix product of a linear system

$$\mathbf{P_{z_m}}=\mathbf{H_{\Delta z}}\mathbf{P_{z_c}}, \tag{13}$$

where $\mathbf{H_{\Delta z}}$, $\mathbf{P_{z_m}}$ are known and $\mathbf{P_{z_c}}$ is to be calculated. $\mathbf{P_{z_m}}$ and $\mathbf{P_{z_c}}$ are time-dependent column vectors composed of the wavenumber spectrum values at the positions $z=z_m$ and $z=z_c$ for the couple $\left(k_{x_i},k_{y_j}\right)$. $\mathbf{H_{\Delta z}}$ is a Toeplitz matrix depending on the propagation distance Δz whose components $h_{i,j}(n)$ are the values of the impulse response $h(k_x, k_y, \Delta z, t)$ for $k_x=k_{x_i}$ and $k_y=k_{y_i}$ at time $t=n\Delta t$. According to Eq. (4), the impulse response $h(k_x, k_y, \Delta z, t)$ is equal to zero for $t<\tau$. $\tau=\Delta z/c$ corresponds to the time needed for the waves to propagate from the plane $z=z_c$ to the measurement plane $z=z_m$. By considering n_τ the smallest sample for which $\tau\le n_\tau\times T_e$, where T_e is the sampling period, Eq. (13) can be formulated as

$$\begin{bmatrix}P_{ij}(n_\tau)\\ \vdots\\ \vdots\\ \vdots\\ P_{ij}(N-1)\end{bmatrix}_{z_m}=\begin{bmatrix}h_{ij}(n_\tau) & 0 & \cdots & \cdots & 0\\ \vdots & \ddots & \ddots & & \vdots\\ \vdots & & \ddots & \ddots & \vdots\\ \vdots & & & \ddots & 0\\ h_{ij}(N-1) & \cdots & \cdots & \cdots & h_{ij}(n_\tau)\end{bmatrix}_{\Delta z}\times\begin{bmatrix}P_{ij}(0)\\ \vdots\\ \vdots\\ \vdots\\ P_{ij}(N-1-n_\tau)\end{bmatrix}_{z_c}. \tag{14}$$

Vectors $\mathbf{P_{z_m}}$ and $\mathbf{P_{z_c}}$ have $(N-n_\tau)$ components. $\mathbf{H_{\Delta z}}$ is a $(N-n_\tau)\times(N-n_\tau)$ square matrix. N is the number of time samples considered for the discrete impulse response. The standard Tikhonov regularized solution $\mathbf{P}^{\lambda}_{\mathbf{z_c}}$ of Eq. (13) is given by

$$\mathbf{P}^{\lambda}_{\mathbf{z_c}}=\mathbf{arg}\min_{\mathbf{P_{z_c}}}\left\{\|\mathbf{H_{\Delta z}}\mathbf{P_{z_c}}-\mathbf{P_{z_m}}\|_2^2+\lambda\|\mathbf{P_{z_c}}\|_2^2\right\}, \tag{15}$$

where $\left\|\mathbf{P_{z_c}}\right\|_2^2$ is the $L2$ norm of $\mathbf{P_{z_c}}$ and λ is the regularization parameter which will influence the weight of the regularization.

After constituting the vector $\mathbf{P_{z_m}}$ with the time-dependent wavenumber spectrum of the hologram $P(k_x, k_y, z_m, t)$, the standard Tikhonov regularization is applied for each pair $\left(k_{x_i},k_{y_j}\right)$ using the singular value decomposition (SVD) of matrix $\mathbf{H_{\Delta z}}$

$$\mathbf{H_{\Delta z}}=\mathbf{USV^H}, \tag{16}$$

where $\mathbf{S}$ is the diagonal matrix of the singular values s_i, $i=1\ldots L$, $(L=N-n_\tau)$ of $\mathbf{H_{\Delta z}}$, $\mathbf{S}$ and $\mathbf{V}$ are the singular orthonormal matrices associated. $\mathbf{V^H}$ is the transconjugate of matrix $\mathbf{V}$. The inverse of $\mathbf{H_{\Delta z}}$ is

$$\mathbf{H^{-1}_{\Delta z}}=\left(\mathbf{USV^H}\right)^{-1}=\mathbf{VS^{-1}U^H}, \tag{17}$$

$$\mathbf{H^{-1}_{\Delta z}}=\mathbf{V}\,\mathbf{diag}\left(\frac{1}{s_1},\cdots,\frac{1}{s_L}\right)\mathbf{U^H}. \tag{18}$$

The nonregularized solution of Eq. (13) can be written as

$$\mathbf{P_{z_c}}=\sum_{i=1}^{L}\frac{\mathbf{u_i^H}\mathbf{P_{z_m}}}{s_i}\mathbf{v_i}. \tag{19}$$

The regularization acts as a filter on the singular values s_i of $\mathbf{H_{\Delta z}}$, yielding the regularized solution

$$\mathbf{P}^{\lambda}_{\mathbf{z_c}}=\sum_{i=1}^{L}f_i\frac{\mathbf{u_i^H}\mathbf{P_{z_m}}}{s_i}\mathbf{v_i}, \tag{20}$$

where f_i are the coefficients of the regularization filter. In the case of standard Tikhonov regularization, the filter coefficients f_i are

$$f_i=\frac{s_i^2}{s_i^2+\lambda}. \tag{21}$$

The generalized crossed validation[7] is used to determine the optimal regularization parameter λ. This method consists in minimizing the function G defined by

$$G=\frac{\left\|\mathbf{H_{\Delta z}}\mathbf{P}^{\lambda}_{\mathbf{z_c}}-\mathbf{P_{z_m}}\right\|_2^2}{\left[\mathrm{trace}\left(\mathbf{I}-\mathbf{H_{\Delta z}}\mathbf{H^{-1}_{\Delta z,\lambda}}\right)\right]^2}, \tag{22}$$

where $\mathbf{I}$ is the identity matrix and $\mathbf{H^{-1}_{\Delta z,\lambda}}$ is the regularized inverse of $\mathbf{H_{\Delta z}}$ such as

$$\mathbf{P}_{\mathbf{z_c}}^{\lambda} = \mathbf{H}_{\mathbf{\Delta z},\lambda}^{-\mathbf{1}}\mathbf{P}_{\mathbf{z_m}}. \quad (23)$$

Once the regularization parameters are obtained for each (k_{x_i}, k_{y_j}), the standard Tikhonov regularization [Eq. (20)] is applied yielding the back-propagated time-dependent wavenumber spectrum. Finally, using the inverse two dimensional Fourier transform gives the back propagated time-dependent sound pressure field on the source plane allowing one to characterize and localize the sound sources.

C. Inverse filtering method

The second deconvolution method is based on optimum Wiener filtering.[21] The approach is also detailed in Ref. 12. The searched discrete inverse impulse response $h^{-1}(k_x, k_y, \Delta z, n)$ has to fulfill the equation

$$h^{-1}(k_x, k_y, \Delta z, n) * h(k_x, k_y, \Delta z, n) = \delta(n - N). \quad (24)$$

The delay in the right part ensures the causality of the inverse impulse response $h^{-1}(k_x, k_y, \Delta z, n)$. It is linked to the number of samples N used for $h^{-1}(k_x, k_y, \Delta z, n)$. The solution $h^{-1}(k_x, k_y, \Delta z, n)$ is given by minimizing the mean square error criterion defined as

$$J(k_x, k_y, \Delta z) = \sum_{n=-\infty}^{+\infty} \left[\delta(n - N) - h(k_x, k_y, \Delta z, n) * h^{-1}(k_x, k_y, \Delta z, n)\right]^2. \quad (25)$$

Assuming that the solution is the impulse response of a finite impulse response filter of N samples, Eq. (25) yields

$$J(k_x, k_y, \Delta z) = \sum_{n=-\infty}^{+\infty} \left[\delta(n - N) - \sum_{m=0}^{N-1} h^{-1}(k_x, k_y, \Delta z, m) \times h(k_x, k_y, \Delta z, n - m)\right]^2. \quad (26)$$

The solution is given in a matrix formalism by

$$\mathbf{h_{inv}} = \Phi_{\mathbf{h}}^{-\mathbf{1}}\mathbf{h^r}, \quad (27)$$

where $\mathbf{h_{inv}}$ is the vector of the solutions, Φ_h the correlation matrix of the direct filter and $\mathbf{h^r}$ the reverse vector of the direct filter [$\mathbf{h}(n) = \mathbf{h^r}(N\text{-}1\text{-}n)$, $n = 0, N - 1$]. The components of vector $\mathbf{h_{inv}}$ build the inverse impulse response $h^{-1}(k_x, k_y, \Delta z, n)$. The inverse filter is causal but yields a delay for the response which depends on the number of samples of the impulse direct response.

IV. NUMERICAL SIMULATIONS

A. Setup

The setup of the numerical simulations is shown in Fig. 1. The source plane is composed of three monopoles chosen for their nonstationary properties. M_1 (0.3, 0.4, and 0 m), M_2 (0.7, 0.7, and 0 m) generate a signal with a linear frequency modulation, and M_3 (0.3, 0.7, and 0 m) radiates a Morlet wavelet defined by

$$s(t) = \cos(2\pi f_0 t)e^{-t^2/2}, \quad (28)$$

with $f_0 = 800$ Hz. The simulation of the acquisition is done using a 11×11 microphone array with a step size in both x and y directions $a = 0.1$ m providing an overall scan area of 1.0×1.0 m^2. Signals are simulated on 256 time samples with a sampling frequency $f_s = 16\,000$ Hz. The pressure radiated by the monopoles and recorded by the array at a distance R is $p(t) = s(t - R/c)/R$. Integrating the quadratic pressure during the time duration $T = 16$ ms yields the energy E defined as

$$E = \frac{4\pi}{\rho c}\int_0^T s^2(t)dt, \quad (29)$$

where ρ is the air density. The energies driven by monopoles M_1, M_2, and M_3 are respectively, about 0.021, 0.023, and 0.012 J. The first step is to simulate the acquisition of the time-dependent sound pressure field on the calculation plane $p(x, y, z_c, t)$ with $z_c = 0.05$ m, which is considered as the reference, and on the measurement plane $p(x, y, z_m, t)$ with $z_m = 0.1575$ m. The time-dependent sound pressure field on the measurement plane is then back-propagated using the processed impulse response and the two inversion methods presented earlier in the paper. For the method based on optimum Wiener filtering, the time-dependent reconstructed signals are time-compensated for the comparisons. Figure 4 highlights the time-dependent back-propagated signals in locations R_2, R_3, and R_4, for both inversion methods when the impulse response is processed using Chebyshev filtering. The waveforms obtained indicate that the reconstructed pressure signals are close to the reference signals for the studied locations.

B. Indicators for comparison

In order to compare the relevance of the different processing methods applied to the impulse response to provide the reconstructed pressure time signals, two time indicators T_1 and T_2 are calculated for a point (x_i, y_j) of the source plane facing the area scanned by the microphone array. They are defined by

$$T_1(x_i, y_j) = \frac{< p_{\text{ref}}(x_i, y_j, z_c, t)p(x_i, y_j, z_c, t) >}{\sqrt{< p_{\text{ref}}^2(x_i, y_j, z_c, t) >< p^2(x_i, y_j, z_c, t) >}}, \quad (30)$$

$$T_2(x_i, y_j) = \frac{\left|p_{\text{ref}}^{\text{rms}}(x_i, y_j, z_c) - p^{\text{rms}}(x_i, y_j, z_c)\right|}{p_{\text{ref}}^{\text{rms}}(x_i, y_j, z_c)}, \quad (31)$$

where $p_{\text{ref}}^{\text{rms}}(x_i, y_j, z_c)$ and $p^{\text{rms}}(x_i, y_j, z_c)$ are the root mean square pressure values given by

$$p_{\text{ref}}^{\text{rms}}(x_i, y_j, z_c) = \sqrt{< p_{\text{ref}}^2(x_i, y_j, z_c, t) >}, \quad (32)$$

$$p^{\text{rms}}(x_i, y_j, z_c) = \sqrt{< p^2(x_i, y_j, z_c, t) >}. \quad (33)$$

$\langle\rangle$ is the time averaged value. $p_{\text{ref}}(x_i, y_j, z_c, t)$ is the reference time-dependent pressure signal and $p(x_i, y_j, z_c, t)$ the back-

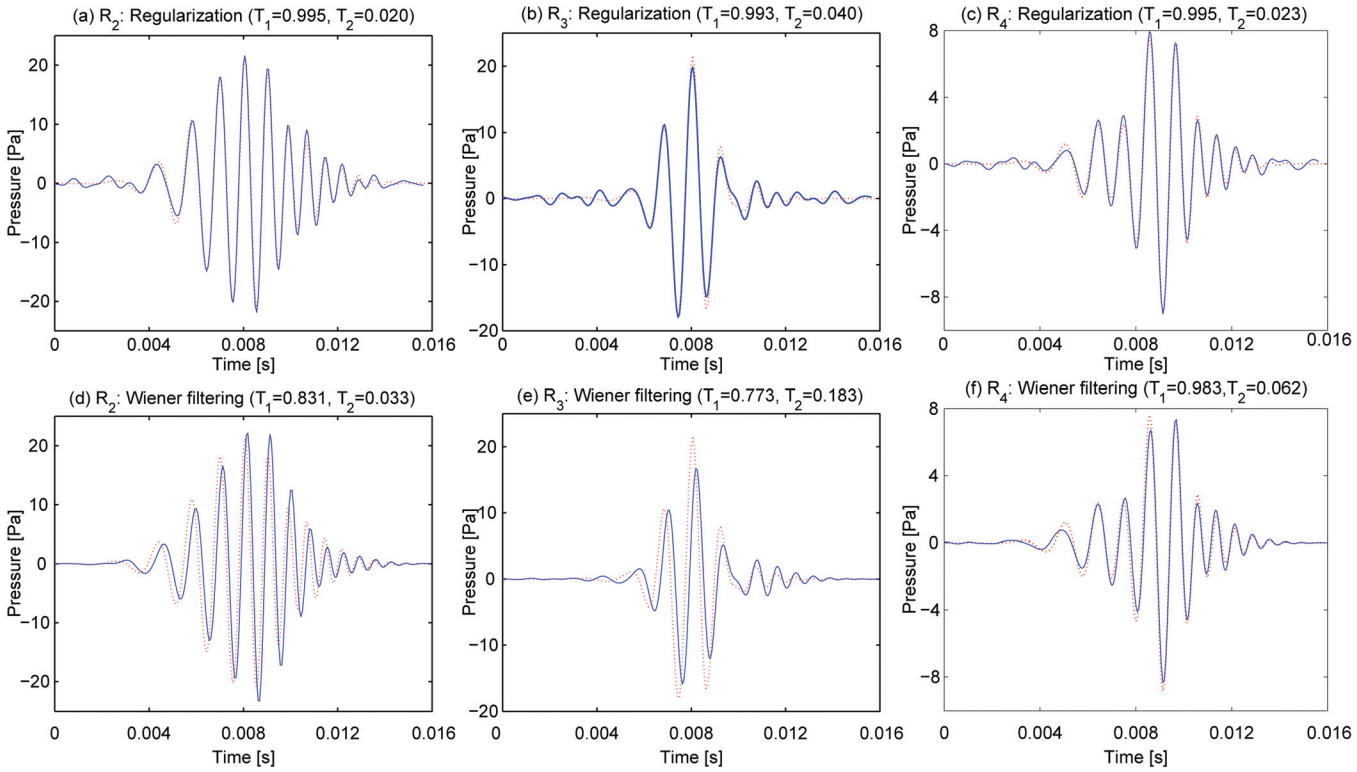

FIG. 4. (Color online) Reconstructed time signals obtained by inverse filtering using singular value decomposition coupled with regularization (a)–(c), or Wiener approach (d)–(f), vs reference signals (dotted line) on locations R_2 [(a), (d)], R_3 [(b), (e)], and R_4 [(c), (f)] (see Fig. 1). The impulse response was processed using Chebyshev low-pass filtering.

propagated time-dependent pressure signal. T_1 is a correlation coefficient which is sensitive to the similarity between the shapes of the signals and thus between their phase difference. The best value for T_1 would be 1. T_2, defined as the relative difference between the root mean square values of the two signals, is also sensitive to the magnitude differences between the reconstructed signals and the references. The target value to reach for T_2 is 0.

TABLE I. Indicator T_1 [see Eq. (30)] computed from reference signals and pressure signals back-propagated to the plane $z = z_c$ in locations R_1, R_2, R_3, and R_4 (see Fig. 1) using the inverse impulse responses obtained by Wiener filtering or regularization from preprocessed impulse responses by the direct method with $f_e = 16\,000$ Hz, the average method, Chebyshev and Kaiser filtering.

	R_1			
	Direct	Average	Chebyshev	Kaiser
Wiener	0.740	0.733	0.796	0.778
Regularization	0.974	0.994	0.994	0.882
	R_2			
	Direct	Average	Chebyshev	Kaiser
Wiener	0.752	0.664	0.831	0.818
Regularization	0.975	0.995	0.995	0.882
	R_3			
	Direct	Average	Chebyshev	Kaiser
Wiener	0.798	0.844	0.773	0.835
Regularization	0.927	0.993	0.993	0.925
	R_4			
	Direct	Average	Chebyshev	Kaiser
Wiener	0.945	0.653	0.983	0.978
Regularization	0.981	0.995	0.995	0.918

C. Results

1. Time-space comparisons

The values of indicators T_1 and T_2 computed at the four positions R_1, R_2, R_3, and R_4, in the case of both inverse methods (Wiener filtering and singular value decomposition coupled with regularization), are shown in Tables I and II. Even if the waveforms shown in Fig. 4

TABLE II. Indicator T_2 [see Eq. (31)] computed from reference signals and pressure signals back-propagated to the plane $z = z_c$ in locations R_1, R_2, R_3, and R_4 (see Fig. 1) using the inverse impulse responses obtained by Wiener filtering or regularization from pre-processed impulse responses by the direct method with $f_e = 16\,000$ Hz, the average method, Chebyshev and Kaiser filtering.

	R_1			
	Direct	Average	Chebyshev	Kaiser
Wiener	0.067	0.251	0.018	0.102
Regularization	0.341	0.019	0.019	0.033
	R_2			
	Direct	Average	Chebyshev	Kaiser
Wiener	0.092	0.255	0.033	0.092
Regularization	0.332	0.020	0.020	0.013
	R_3			
	Direct	Average	Chebyshev	Kaiser
Wiener	0.145	0.361	0.183	0.003
Regularization	0.452	0.040	0.040	0.023
	R_4			
	Direct	Average	Chebyshev	Kaiser
Wiener	0.015	0.165	0.062	0.078
Regularization	0.282	0.024	0.023	0.025

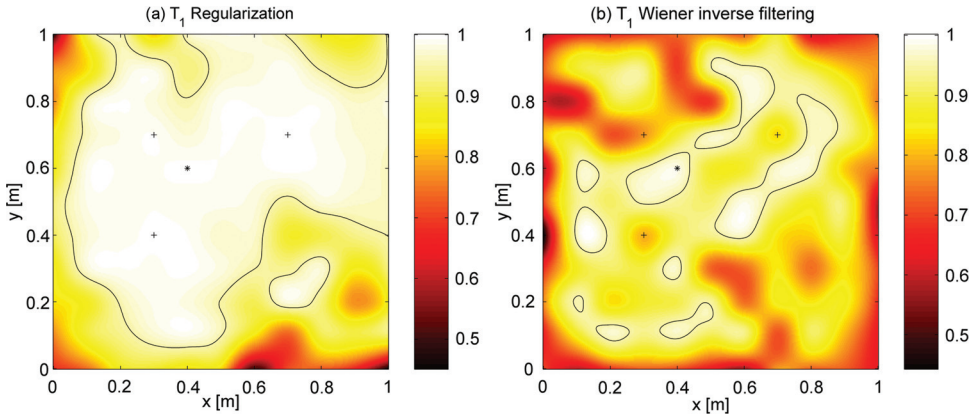

FIG. 5. (Color online) Spatial maps for indicator T_1 in the case of regularization (a) and inverse filtering (b) with a contour line at the value 0.95. The locations of $R_1(+)$, $R_2(+)$, $R_3(+)$, and $R_4(*)$ are marked.

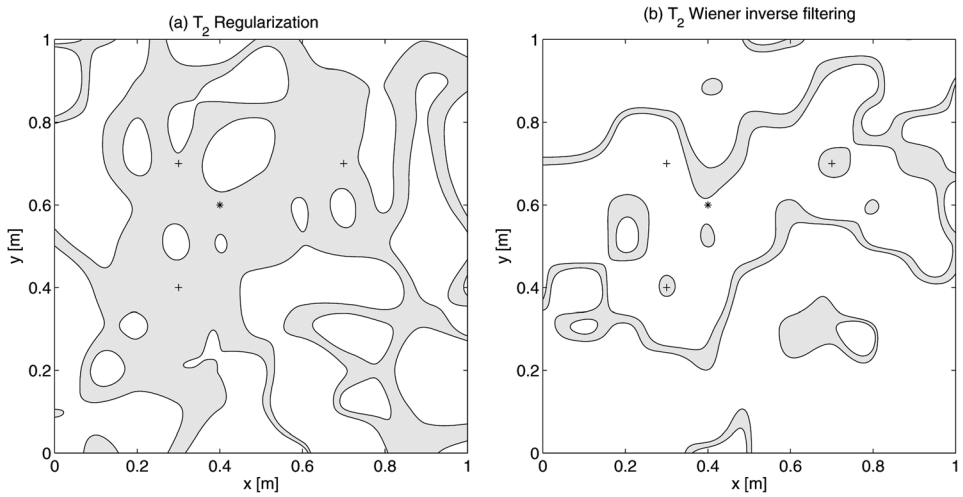

FIG. 6. Spatial maps for indicator T_2 in the case of regularization (a) and inverse filtering (b). The areas in gray correspond to values of T_2 below 0.05. The locations of $R_1(+)$, $R_2(+)$, $R_3(+)$, and $R_4(*)$ are marked.

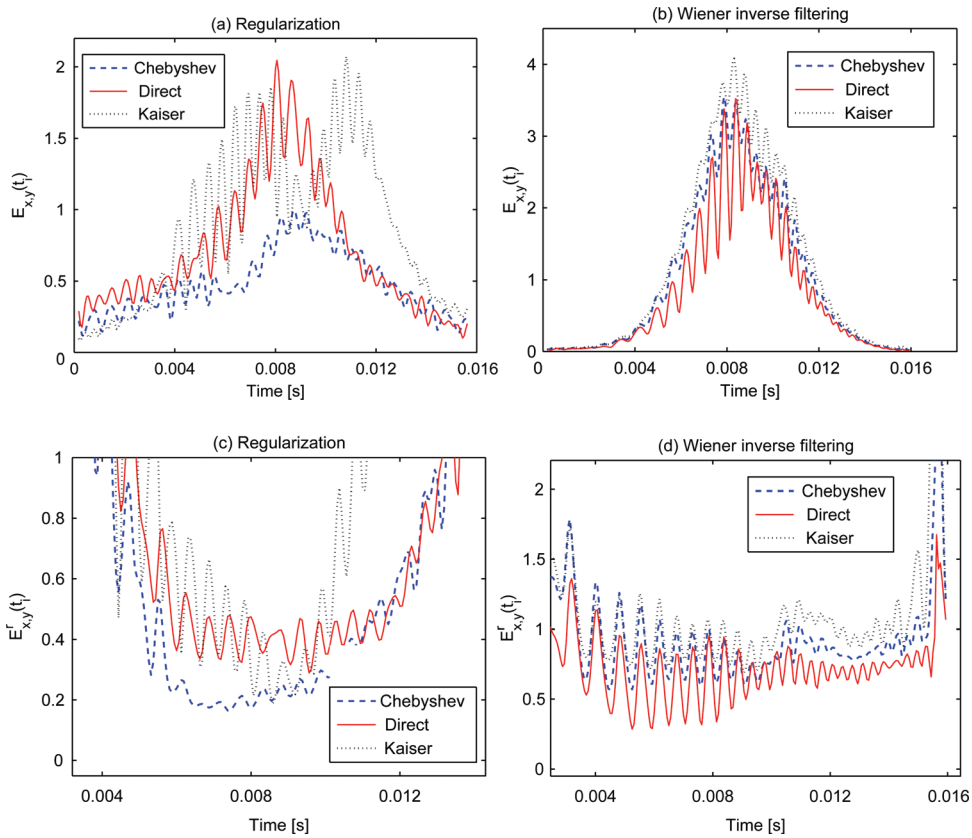

FIG. 7. (Color online) Time-dependent spatial errors $E_{x,y}$ [see Eq. (34)] and $E^r_{x,y}$ [see Eq. (35)] in the case of regularization (a), (c), and inverse filtering (b), (d) for three processing methods applied to the impulse response (direct sampling, Kaiser and Chebyshev filtering).

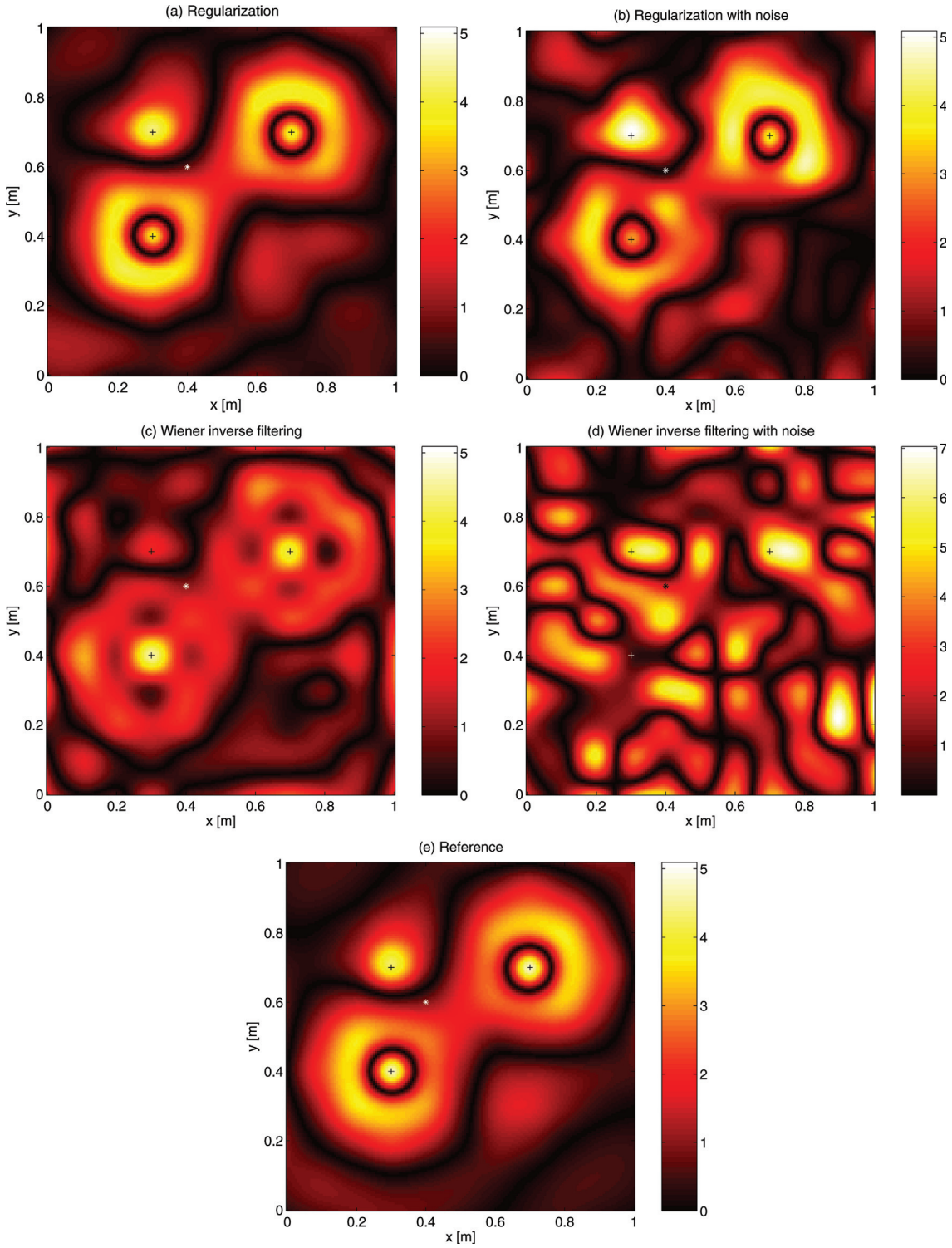

FIG. 8. (Color online) Comparison of the modulus in Pa of spatial sound pressure fields at time $t = 6.2$ ms: The back-propagated spatial sound pressure fields using regularization with (b) or without measurement noise (a), Wiener inverse filtering with (d) or without measurement noise (c), the reference field (e). Inversion is achieved from an impulse response preprocessed by Chebyshev low-pass filtering. In the case of measurement noise, the signal-to-noise ratio (SNR) is 3 dB.

seem satisfactory, the objective indicators T_1 and T_2 are not so good when Wiener filtering is done. In this case and for the locations facing the monopole sources, T_1 shows that processing the impulse response with Chebyshev or Kaiser filtering improves the results. However the direct method gives accurate results in terms of amplitudes (see Table II).

Concerning the inversion methods, it can be noticed according to indicators T_1 and T_2 that the regularization method provides more accurate reconstructed pressure signals than Wiener filtering at the four proposed locations. In order to extend this conclusion to the whole spatial domain it is possible to compute the values of indicators T_1 and T_2 for each location facing the microphone positions. The maps of

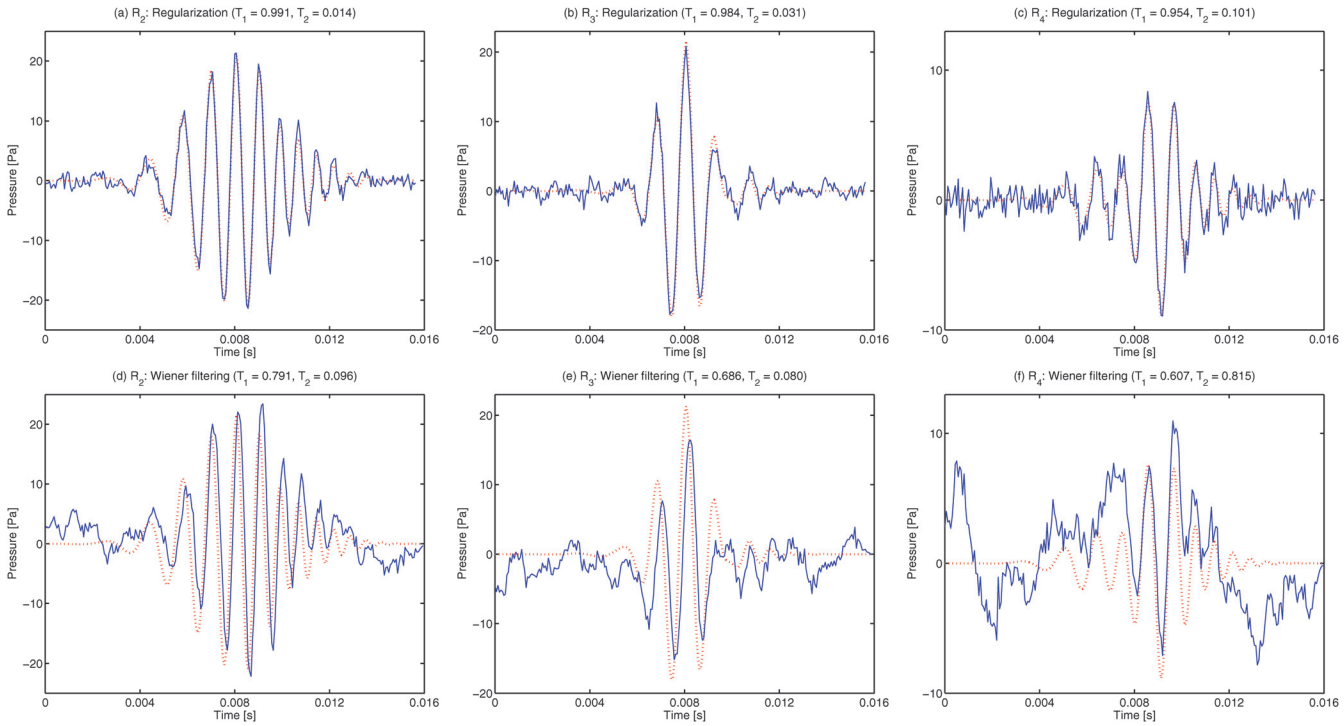

FIG. 9. (Color online) Comparison between reference signals (dotted line) and back-propagated signals using regularization method (a)–(c), and inverse Wiener filtering method (d)–(f), associated with Chebyshev low-pass filtering on locations R_2, R_3, and R_4 with a signal to measurement noise ratio SNR = 3 dB.

indicator T_1 with the 0.95 contour line for both inversion methods in the case of Chebyshev filtering of the impulse response are shown in Fig. 5. The maps of indicator T_2 for both inversion methods in the case of Chebyshev filtering of the impulse response are shown in Fig. 6. The area in gray delimits the spatial locations where indicator T_2 is below 0.05. It is obvious that the use of the regularization inversion method notably improves the reconstructed time-dependent sound pressure field obtained on the whole spatial domain. The examination of the maps, obtained by the four methods tested (only the maps from Chebyshev processing are shown here in Figs. 5 and 6), demonstrated that Chebyshev filtering and the average method, associated with regularization, provide the most accurate results. Thus it confirms the tendencies highlighted by Tables I and II. In the case of Wiener filtering, it seems that the Direct method provides the best results except when the signals are reconstructed in front of the monopole sources. This result was also mentioned in Ref. 12.

2. Spatial comparisons

Indicators T_1 and T_2 describe the quality of the reconstructed temporal signals at a given position. The values of those indicators shown in Figs. 5 and 6 are not constant on the whole spatial domain. In order to evaluate the quality of the reconstruction of the spatial pressure field and thus the relevance of the source localization, two spatial error criteria are introduced, one defined by

$$E_{x,y}(t_i) = \sqrt{< \left[p_{\text{ref}}(x,y,z_c,t_i) - p(x,y,z_c,t_i)\right]^2 >}, \quad (34)$$

which corresponds to the total error between the reference pressure field and the back propagated pressure field at a given time t_i. $\langle\rangle$ is the spatial averaged value. The other criterion is the relative error

$$E^r_{x,y}(t_i) = \frac{E_{x,y}(t_i)}{\left[< p^2_{\text{ref}}(x,y,z_c,t_i) >\right]^{\frac{1}{2}}}, \quad (35)$$

which is suitable to quantify the quality of the reconstruction while the total error is more relevant for comparing the inverting methods. The values of both spatial error criteria, shown in Fig. 7, confirm the advantage of inverting the impulse response using SVD coupled with regularization and that preprocessing the impulse response does not seem useful when using Wiener filtering. High values of the relative spatial error are obtained at the edges of the signal due to the fact that the reference pressure field supplies the denominator of Eq. (35) with very low values at these time intervals. The use of the regularization method with appropriate processing of the impulse response (Chebyshev low-pass filtering here) highly improves the reconstruction of the spatial sound pressure field. This can be also illustrated in Fig. 8 by considering the reconstructed spatial sound pressure field at a given time $t = 6.2$ ms using regularization (a) and inverse filtering (c) associated with Chebyshev filtering versus the reference (e) on the calculation plane.

3. Noise influence

Measurement noise is a key factor in the case of ill-posed problem. Indeed a small variation on the input signal

TABLE III. Indicators T_1 and T_2 [see Eqs. (30) and (31)] computed from reference signals and pressure signals back-propagated to the plane $z = z_c$ in locations R_1, R_2, R_3, and R_4 (see Fig. 1) using the inverse impulse responses obtained by Wiener filtering or regularization in the case of measurement noise with a signal to noise ratio SNR = 3 dB.

	T_1			
	R_1	R_2	R_3	R_4
Wiener	0.779	0.791	0.686	0.607
Regularization	0.990	0.991	0.984	0.954
	T_2			
	R_1	R_2	R_3	R_4
Wiener	0.038	0.096	0.080	0.815
Regularization	0.033	0.014	0.031	0.101

may lead to an important variation on the output signal and thus yields highly unstable solutions. In the presence of measurement noise, the reconstructed signals at R_2, R_3, and R_4 locations on the calculation plane for the regularization method and the inverse filtering method versus reference are shown in Fig. 9. It is noticeable that both inversion methods yields rather stable back-propagated signals. However, the inverse filtering method appears to be more sensitive to the measurement noise as shown by the indicators T_1 and T_2 reported in Table III. This is also true in Fig. 8 where the spatial pressure field is reconstructed in the presence of measurement noise for both inverse methods based on regularization (b) and on Wiener filtering (d). This can be explained by the fact that the determination of the inverse impulse response with the inverse filtering method is only based on the values of the impulse response h. On the other hand the regularization method and particularly the Generalized Crossed Validation approach takes into account the measured signal with the added measurement noise to calculate the optimal regularization parameter λ. This method thus acts differently depending on the quality of the measured signals. The values of the spatial errors $E_{x,y}$ and $E^r_{x,y}$ are shown in Fig. 10. The conclusion given at locations R_2, R_3, and R_4 can be extended to the whole spatial domain of the antenna. The regularization method highly decreases the influence of the measurement noise especially when the sound sources are active.

V. CONCLUSION

At least two methods are suitable for effectively implementing real-time near-field acoustic holography and particularly for solving the inverse problem, that is, reconstructing the time-dependent sound field on the source plane from measurements acquired using a microphone array in the near-field. The aim of both methods is to invert an impulse response. A simulation involving monopoles driven by nonstationary signals showed that the first method based on Wiener filtering can directly work on the discretized impulse response which needs no pre-processing except for specific location facing the monopole sources for which upsampling and Chebyshev low-pass filtering improved the reconstruction. The second method performs the inversion of the direct impulse response by using singular value decomposition coupled with regularization. The study shows that regularization enhances the results according to objective indicators by improving the shapes and the amplitudes of the

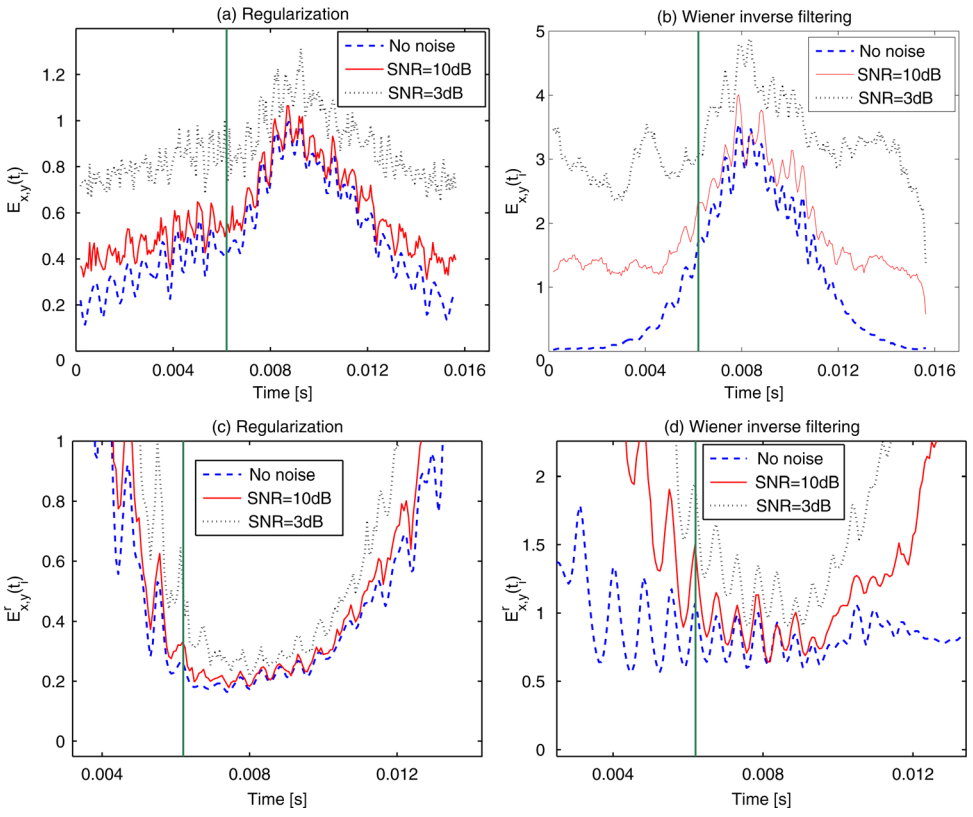

FIG. 10. (Color online) Noise influence on the spatial errors $E_{x,y}$ and $E^r_{x,y}$ in the case of regularization (a), (c) and inverse filtering (b), (d) when Chebyshev filtering is applied to the impulse response. The vertical line indicates the time chosen ($t = 6.2$ ms) for the spatial field representation in Fig. 8.

reconstructed time-dependent acoustic signals on the backward plane. In addition, the second method with regularization appears to be less sensitive to measurement noise than Wiener filtering. Thus, the inverting process based on singular value decomposition coupled with regularization is more advantageous than Wiener filtering for accurately reconstructing nonstationary acoustic fields, especially in the presence of noise.

These inverse processing methods make RT-NAH very promising to monitor and diagnose the behavior of time-evolving acoustic systems. Indeed RT-NAH has the ability to continuously provide accurate time-dependent pressure signal on the source plane as if the microphones were embedded into the sources.

[1]E. G. Williams, *Fourier Acoustics: Sound Radiation and Nearfield Acoustical Holography* (Academic, New York, 1999), pp. 89–114.

[2]J. Hald, "Time domain acoustical holography," in Proceedings of Inter-noise, Newport Beach (July, 1995), pp. 1349–1354.

[3]J. Hald, *Non stationary STSF* (Brüel & Kjaer Technical Review, Naerum, Denmark, 2000), pp. 1–36.

[4]J. Hald, "Time domain acoustical holography and its applications," Sound Vib. **35**, 16–25 (2001).

[5]O. de La Rochefoucauld-Rossier, "Résolution du problème inverse spatio-temporel en imagerie acoustique de champ proche: Application au rayonnement de sources industrielles instationnaires (Solving the space-time inverse problem in near-field acoustic imaging: Application to non-stationary radiating sources in industry)," Ph.D. dissertation, Université du Maine, Le Mans, France, pp. 1–175 (2002).

[6]O. de la Rochefoucauld, M. Melon, and A. Garcia, "Time domain holography: forward projection of simulated and measured sound pressure fields," J. Acoust. Soc. Am. **116**(2), 142–153 (2004).

[7]P. C. Hansen. *Rank-Deficient and Discrete Ill-Posed Problems* (SIAM, Philadelphia, 1998), pp. 1–247.

[8]J.-F. Blais and A. Ross, "Backward propagation of sound fields radiated by impacted plates using a transient acoustical holography approach," in *Proceedings of Inter-noise*, Ottawa, Canada (August, 2009), paper 916.

[9]J.-F. Blais and A. Ross, "Forward projection of transient sound pressure fields radiated by impacted plates using numerical laplace transform," J. Acoust. Soc. Am. **125**(5), 3120–3128 (2009).

[10]S. F. Wu, H. Lu, and M. S. Bajwa, "Reconstruction of transient acoustic radiation from a sphere," J. Acoust. Soc. Am. **117**(4), 2065–2077 (2005).

[11]F. Deblauwe, J. Leuridan, J. L. Chauray, and B. Béguet, "Acoustic holography in transient conditions," in *Proceedings of the Sixth International Congress on Sound and Vibration*, Copenhagen, Denmark (July, 1999), pp. 899–906.

[12]J.-H. Thomas, V. Grulier, S. Paillasseur, J.-C. Pascal, and J.-C. Le Roux, "Real-Time near-field acoustic holography for continuously visualizing nonstationary acoustic fields," J. Acoust. Soc. Am. **128**(6), 3554–3567 (2010).

[13]S. Paillasseur, "Développement de la technique d'holographie acoustique de champ proche temps-réel pour l'analyse de sources de bruit fluctuantes (Improvement of the real-time near-field acoustic holography technique for analyzing fluctuating acoustic sources)," Ph.D. dissertation, Université du Maine, Le Mans, France, pp. 1–130 (2009).

[14]M. Forbes, S. Letcher, and P. Stepanishen, "A wave vector, time-domain method of forward projecting time-dependent pressure fields," J. Acoust. Soc. Am. **90**(5), 2782–2792 (1991).

[15]V. Grulier, S. Paillasseur, J.-H. Thomas, J.-C. Pascal, and J.-C. Le Roux, "Forward propagation of time evolving acoustic pressure: Formulation and investigation of the impulse response in time-wavenumber domain," J. Acoust. Soc. Am. **126**(5), 2367–2378 (2009).

[16]E. G. Williams, "Regularization methods for near-field acoustical holography," J. Acoust. Soc. Am. **110**(4), 1976–1988 (2001).

[17]V. Grulier, "Propagation directe, inverse dans l'espace temps-nombre d'onde: application à une méthode d'holographie acoustique de champ proche pour les sources non stationnaires (Direct et inverse propagation in the time-wavenumber domain: application to a near-field acoustic holography method for nonstationary sources)," Ph.D. dissertation, Université du Maine, Le Mans, France, pp. 1–121 (2005).

[18]M. R. Bai, "Acoustical source characterization by using recursive Wiener filtering," J. Acoust. Soc. Am. **97**(5), 2657–2663 (1995).

[19]J. F. Li, J.-C. Pascal, and C. Carles, "A new k-space optimal filter for acoustic holography," in *Proceedings of the Third International Congress on Air and Structure Borne Sound and Vibration*, Montreal, Canada (June, 1994), pp. 1059–1066.

[20]A. Tikhonov, "Solutions of incorrectly formulated problems and the regularization method," Sov. Math. Dokl. **4**, 1035–1038 (1963).

[21]S. Haykin, *Adaptive Filter Theory*, 3rd ed. (Prentice Hall, Englewood Cliffs, NJ, 1996), pp. 1–989.